Low-frequency logarithmic discretization of the reservoir spectrum for improving the efficiency of hierarchical equations of motion approach

LvZhou Ye,[1] Hou-Dao Zhang,[2,a)] Yao Wang,[1] Xiao Zheng,[1,3,b)] and YiJing Yan[1,4]
[1]*Hefei National Laboratory for Physical Sciences at the Microscale, University of Science and Technology of China, Hefei, Anhui 230026, China*
[2]*Department of Chemical Physics, University of Science and Technology of China, Hefei, Anhui 230026, China*
[3]*Synergetic Innovation Center of Quantum Information and Quantum Physics, University of Science and Technology of China, Hefei, Anhui 230026, China*
[4]*iChEM (Collaborative Innovation Center of Chemistry for Energy Materials), University of Science and Technology of China, Hefei, Anhui 230026, China*

(Received 18 May 2017; accepted 4 August 2017; published online 17 August 2017)

An efficient low-frequency logarithmic discretization (LFLD) scheme for the decomposition of fermionic reservoir spectrum is proposed for the investigation of quantum impurity systems. The scheme combines the Padé spectrum decomposition (PSD) and a logarithmic discretization of the residual part in which the parameters are determined based on an extension of the recently developed minimum-dissipaton ansatz [J. J. Ding *et al.,* J. Chem. Phys. **145**, 204110 (2016)]. A hierarchical equations of motion (HEOM) approach is then employed to validate the proposed scheme by examining the static and dynamic system properties in both the Kondo and noninteracting regimes. The LFLD scheme requires a much smaller number of exponential functions than the conventional PSD scheme to reproduce the reservoir correlation function and thus facilitates the efficient implementation of the HEOM approach in extremely low temperature regimes. *Published by AIP Publishing.* [http://dx.doi.org/10.1063/1.4999027]

I. INTRODUCTION

Quantum impurity models are widely adopted for the development of various methods to tackle strongly correlated electron problems. At the heart of these methods lies the accurate and efficient characterization of correlated electronic states in the presence of dissipative environments and external fields. This is a challenging but rewarding task. Enormous theoretical efforts have been made to accomplish this goal, including the numerical renormalization group method,[1,2] the density-matrix renormalization group method,[3] the quantum Monte Carlo approach,[4,5] the exact diagonalization method,[6] the real-time path integral method,[7,8] and the multilayer multiconfiguration time-dependent Hartree method.[9,10] However, the validity and practicality of these methods are usually restricted to a limited parameter space and some basic models.

In the past decades, the hierarchical equations of motion (HEOM) approach has been developed for the accurate and universal characterization of general open quantum systems.[11–42] It has been employed to investigate various static and dynamic processes in strongly correlated electronic systems for both equilibrium and nonequilibrium situations, such as the dynamical Kondo transition,[21] the Kondo phenomena in adsorbed and mechanically stretched magnetic molecules,[43–46] the Mott-Hubbard metal-insulator transition of lattice models,[47] the thermoelectric and local heating effects in quantum dots,[48–50] and the charge transport in nanosystems with strong electronic-vibrational coupling.[51]

The extent of the HEOM is characterized by two parameters:[39] the truncation tier level, L, and the number of the exponential functions to expand the reservoir correlation functions, M. The evaluation of low-temperature properties of strongly correlated systems usually requires large L and M. This makes the HEOM calculations prohibitively expensive and thus poses a major challenge for the present HEOM approach. For the time being, the HEOM-based studies at extremely low temperatures can only be carried out on the noninteracting systems, where L can be relatively small.[39] However, a large M is still needed for the accurate approximation of the reservoir correlation functions. In this situation, the numerical efficiency of HEOM is severely dependent on the scheme for decomposing the reservoir correlation function,[21,52–54] as will be shown in Sec. II. At a low temperature, the computational cost substantially increases because a rather large size of memory basis set is required to expand the reservoir correlation function. This is a major bottleneck hindering the investigation of strong correlation effects in low temperature regimes. Therefore, novel decomposition schemes that can reproduce the reservoir correlation function with a relatively small size of basis set are highly desirable. Recently a minimum-dissipaton ansatz on bath correlation function has been proposed for the bosonic HEOM formalism.[54,55] In this work, we focus on the memory decomposition of the fermionic environments with a low-frequency logarithmic

a)hdz@ustc.edu.cn
b)xz58@ustc.edu.cn

discretization (LFLD) scheme. This scheme significantly reduces the size of the memory basis set and thus facilitates the efficient implementation of HEOM in extremely low temperature regimes.

The remainder of this paper is organized as follows. In Sec. II, the single-impurity Anderson model is introduced and the decomposition of the reservoir correlation function and construction of the HEOM formalism are briefly discussed. The proposed LFLD scheme for the decomposition of the reservoir spectrum is presented in Sec. III. In Sec. IV, we demonstrate the efficiency and accuracy of the proposed scheme via numerical simulations in low temperature regimes. Concluding remarks are finally given in Sec. V.

II. ANDERSON IMPURITY MODEL AND HEOM APPROACH

In this work, we consider a single-impurity Anderson model. The quantum impurity system is described by $H_{\rm sys} = \epsilon_d(\hat{n}_\uparrow + \hat{n}_\downarrow) + U\hat{n}_\uparrow\hat{n}_\downarrow$. Here, $\hat{n}_s = \hat{a}_s^\dagger\hat{a}_s$, with $\hat{a}_s^\dagger$ ($\hat{a}_s$) creating (annihilating) a spin-s ($s = \uparrow$ or $\downarrow$) electron on energy level ϵ_d, and U is the Coulomb repulsion strength. The total Hamiltonian is $H_{\rm total} = H_{\rm res} + H_{\rm sys} + H_{\rm sys\text{-}res}$, with $H_{\rm res} = \sum_{\alpha k}(\epsilon_{\alpha k} + V_\alpha)\hat{d}_{\alpha k}^\dagger\hat{d}_{\alpha k}$ and $H_{\rm sys\text{-}res} = \sum_{\alpha\nu k_s} t_{\alpha\nu k}\hat{a}_s^\dagger\hat{d}_{\alpha k} + {\rm H.c.}$, for the non-interacting reservoirs and system-reservoir couplings, respectively. Here, V_α is a homogeneous energy shift for the states in α-reservoir; $\hat{d}_{\alpha k}^\dagger$ ($\hat{d}_{\alpha k}$) is the creation (annihilation) operator for the α-reservoir state $|k\rangle$ of energy $\epsilon_{\alpha k}$, and $t_{\alpha\nu k}$ is the coupling strength between system level state ν and α-reservoir single-electron state of wavevector $|k\rangle$. The influences of reservoirs on the system are characterized by the reservoir spectral function $J_{\alpha\nu\nu'}(\omega) = \pi\sum_k t_{\alpha\nu k}t_{\alpha\nu' k}^*\delta(\omega - \epsilon_{\alpha k} - V_\alpha)$.

The system-reservoir coupling Hamiltonian is accounted for the reservoir correlation function

$$C_{\alpha\nu\nu'}^\sigma(t,\tau) = \exp\left\{\sigma i\int_\tau^t dt'\, V_\alpha(t')\right\} C_{\alpha\nu\nu'}^{\sigma,{\rm eq}}(t-\tau), \quad (1)$$

$$C_{\alpha\nu\nu'}^{\sigma,{\rm eq}}(t) = \frac{1}{\pi}\int_{-\infty}^{\infty} d\omega\, e^{\sigma i\omega t} f_\alpha^\sigma(\omega) J_{\alpha\nu\nu'}^\sigma(\omega). \quad (2)$$

Here, $C_{\alpha\nu\nu'}^{\sigma,{\rm eq}}(t-\tau)$ is the reservoir correlation function at equilibrium; $V_\alpha(t)$ is the time-dependent bias voltage applied to α-reservoir; $f_\alpha^\sigma(\omega) = 1/[1+e^{\sigma\beta_\alpha(\omega-\mu^{\rm eq})}]$ is the Fermi function for electron ($\sigma = +$) or hole ($\sigma = -$) at the inverse temperature $\beta_\alpha = 1/(k_B T_\alpha)$ and under the equilibrium chemical potential $\mu^{\rm eq}$; $\bar{\sigma} = -\sigma$, and $J_{\alpha\nu\nu'}^-(\omega) \equiv J_{\alpha\nu\nu'}(\omega) = J_{\alpha\nu'\nu}^*(\omega) = J_{\alpha\nu'\nu}^+(\omega)$. For an illustration, we consider the reservoir spectral density function in the form of

$$J_{\alpha\nu\nu'}(\omega) = \frac{\Delta_{\alpha\nu\nu'}W^2}{\omega^2 + W^2}. \quad (3)$$

Here, W is the reservoir bandwidth and $\Delta_{\alpha\nu\nu'}$ is the effective system-reservoir coupling strength. Throughout the paper, we set $\hbar = k_B = e = 1$ and $\mu^{\rm eq} = 0$.

To construct the formally closed HEOM, we expand the reservoir correlation function by a series of exponential functions

$$C_{\alpha\nu\nu'}^{\sigma,{\rm eq}}(t) \simeq \sum_{m=1}^M \eta_{\alpha\nu\nu' m}^\sigma e^{-\gamma_{\alpha m}^\sigma t}, \quad (4)$$

which serve as the basis set that resolves the non-Markovian memory of the fermionic environment. For the form of spectral density adopted in Eq. (3), $\gamma_{\alpha m}^\sigma$ is independent of ν and ν'. Various schemes have been proposed to determine the expansion coefficients $\{\eta_{\alpha\nu\nu' m}^\sigma\}$ and exponents $\{\gamma_{\alpha m}^\sigma\}$. These include the Matsubara spectrum decomposition (MSD) scheme,[16,17,20] a hybrid spectrum decomposition and frequency dispersion scheme,[21] the partial fractional decomposition scheme,[56] and the Padé spectrum decomposition (PSD) scheme.[24,52,53] The number of exponential functions M determines the size of the memory basis set for the decomposition of $C_{\alpha\nu\nu'}^{\sigma,{\rm eq}}(t)$ and further the numerical efficiency of HEOM simulations. Therefore, a spectrum decomposition scheme that minimizes M is highly desirable. So far, the PSD scheme has proved to be superior to any other existing scheme, where the Fermi function is expanded by[24,53]

$$f_\alpha^\sigma(\omega) \simeq \frac{1}{2} - \sigma\frac{\omega}{\beta_\alpha}\sum_{p=1}^P \frac{2\tilde{\eta}_p}{\omega^2 + \tilde{\xi}_p^2}. \quad (5)$$

Here, the parameters $\{\tilde{\eta}_p\}$ and $\{\tilde{\xi}_p\}$ are all positive real numbers and can be obtained with high precision.[24,53]

With the exponential decomposition of the reservoir correlation function, the final HEOM can be cast into a compact form as[20,28,39,40]

$$\dot{\rho}_{j_1\cdots j_n}^{(n)} = -\Big(i\mathcal{L} + \sum_{r=1}^n \gamma_{j_r}\Big)\rho_{j_1\cdots j_n}^{(n)} - i\sum_j \mathcal{A}_{\bar{j}}\,\rho_{j_1\cdots j_n j}^{(n+1)} - i\sum_{r=1}^n (-)^{n-r}\,\mathcal{C}_{j_r}\,\rho_{j_1\cdots j_{r-1}j_{r+1}\cdots j_n}^{(n-1)}. \quad (6)$$

Here, $\rho^{(0)}(t) = \rho(t) \equiv {\rm tr}_{\rm res}\,\rho_{\rm total}(t)$ is the reduced density matrix, and $\{\rho_{j_1\cdots j_n}^{(n)}(t); n = 1,\cdots,L\}$ are the auxiliary density operators (ADOs), with L denoting the truncation level. The multi-component index $j \equiv (\sigma\alpha\nu\nu' m)$ characterizes the transfer of an electron from/to ($\sigma = +/-$) the impurity level-ν to/from level-ν' via the αth reservoir and associated with a characteristic memory time $(\gamma_{\alpha m}^\sigma)^{-1}$. The Grassmann superoperators $\mathcal{A}_{\bar{j}} \equiv \mathcal{A}_\nu^{\bar{\sigma}}$ and $\mathcal{C}_j \equiv \mathcal{C}_{\alpha\nu\nu' m}^\sigma$ are defined via $\mathcal{A}_\nu^{\bar{\sigma}}\hat{O}_\pm \equiv [\hat{a}_\nu^{\bar{\sigma}}, \hat{O}_\pm]_\pm$ and $\mathcal{C}_{\alpha\nu\nu' m}^\sigma\hat{O}_\pm \equiv \eta_{\alpha\nu\nu' m}^\sigma\hat{a}_{\nu'}^\sigma\hat{O}_\pm \mp (\eta_{\alpha\nu\nu' m}^{\bar{\sigma}})^*\hat{O}_\pm\hat{a}_{\nu'}^\sigma$, respectively. Here, $\hat{O}_\pm$ denotes an arbitrary operator, with even (+) or odd (−) fermionic parity such as $\rho^{(2m)}$ or $\rho^{(2m+1)}$ in Eq. (6), respectively. The electron-electron interactions are contained in the Liouvillian of impurities, $\mathcal{L}\star \equiv [H_{\rm sys}, \star]$. The expectation of any system observable $\hat{O}$ can be computed via $O = {\rm tr}(\hat{O}\rho)$, and the time-dependent current from α-reservoir to the system is $I_\alpha(t) = -2{\rm Im}\sum_{\nu s m}{\rm tr}[\hat{a}_{\nu s}\rho_{\alpha\nu m}^+(t)]$, with $\left\{\rho_{j_1}^{(1)} = \rho_{\alpha\nu m}^\sigma\right\}$ being the first-tier ADOs.

III. LOW-FREQUENCY LOGARITHMIC DISCRETIZATION SCHEME

In this work, we start from the decomposition of the reservoir correlation function as follows:

$$C_{\alpha\nu\nu'}^{\sigma,{\rm eq}}(t) \equiv C_{\alpha\nu\nu'}^{\sigma,{\rm PSD}}(t) + \delta C_{\alpha\nu\nu'}^{\sigma,{\rm eq}}(t). \quad (7)$$

The PSD-based part $C_{\alpha\nu\nu'}^{\sigma,{\rm PSD}}(t)$ consists of $(P+1)$ exponents, in relation to the P poles from the approximate Fermi function of Eq. (5) and 1 from the spectral density of Eq. (3).

The residual part, $\delta C^{\sigma,\mathrm{eq}}_{\alpha\nu\nu'}(t)$ in Eq. (7), will be constructed in an alternative manner with the following considerations. First of all, the construction of $C^{\sigma,\mathrm{PSD}}_{\alpha\nu\nu'}(t)$ exploits consistently the Padé approximant of the Fermi function, which is used in the evaluation of the pre-exponential coefficient(s) associated with the pole(s) of spectral density function.[24,57] This would effectively correspond to a certain of approximation in the spectral density function. Moreover, the PSD scheme will become expensive in an extremely low temperature regime; see Fig. 4 below. As inferred from the numerical renormalization group methods,[1,2] the reservoir spectral density can be discretized into a set of intervals of which the energy scales follow a logarithmic behavior. This logarithmic discretization scheme effectively accesses the low energy physics, which are important for the impurity properties in the low temperature regime. Drawing on these insights and to sufficiently capture the low-frequency (or equivalently the long-time) features of the reservoirs, we propose the following residual part approximant:

$$\delta C^{\sigma,\mathrm{eq}}_{\alpha\nu\nu'}(t) \simeq \delta C^{\sigma,\mathrm{RP}}_{\alpha\nu\nu'}(t) = \sum_{r=1}^{R} \eta^{\sigma}_{r} e^{-\gamma_r t}, \tag{8}$$

with

$$\log_{10}\frac{\gamma_r}{\bar{\gamma}} = 1 - r. \tag{9}$$

Here, $\bar{\gamma}$ is real and $\eta^{\sigma}_{r} = -(\eta^{\bar{\sigma}}_{r})^{*}$, as inferred from the residual properties.[40] These parameters will be determined based on an extension of the minimum-dissipaton ansatz;[54,55] see Eqs. (14)–(16). The logarithmic form of $\{\gamma_r\}$ is found to be efficient in approximating the residual part $\delta C^{\sigma}_{\alpha\nu\nu'}(t)$ of the reservoir correlation function, as will be shown in Sec. IV. It covers the memory time up to $10^{R-1}/\bar{\gamma}$. Therefore, it is capable of addressing the strong non-Markovian effects on the real-time electron dynamics.

To adequately address the system-reservoir correlations in the long time scale, we propose to determine the parameters $\bar{\gamma}$ and $\{\eta^{\sigma}_{r}\}$ in frequency-domain and introduce the half-space Fourier transforms

$$\hat{C}^{\sigma,\mathrm{eq}}_{\alpha\nu\nu'}(\omega) = \int_0^\infty dt\, e^{\bar{\sigma} i\omega t} C^{\sigma,\mathrm{eq}}_{\alpha\nu\nu'}(t), \tag{10}$$

$$\hat{C}^{\sigma,\mathrm{PSD}}_{\alpha\nu\nu'}(\omega) = \int_0^\infty dt\, e^{\bar{\sigma} i\omega t} C^{\sigma,\mathrm{PSD}}_{\alpha\nu\nu'}(t), \tag{11}$$

$$\delta\hat{C}^{\sigma,\mathrm{eq}}_{\alpha\nu\nu'}(\omega) = \int_0^\infty dt\, e^{\bar{\sigma} i\omega t} \delta C^{\sigma,\mathrm{eq}}_{\alpha\nu\nu'}(t), \tag{12}$$

$$\delta\hat{C}^{\sigma,\mathrm{RP}}_{\alpha\nu\nu'}(\omega) = \int_0^\infty dt\, e^{\bar{\sigma} i\omega t} \delta C^{\sigma,\mathrm{RP}}_{\alpha\nu\nu'}(t). \tag{13}$$

It is easy to verify that $\mathrm{Re}[\hat{C}^{\sigma,\mathrm{eq}}_{\alpha\nu\nu'}(\omega)] = J^{\sigma}_{\alpha\nu\nu'}(\omega) f^{\sigma}_{\alpha}(\omega)$. For any given $\bar{\gamma}$, it is required in this scheme that

$$\delta C^{\sigma,\mathrm{RP}}_{\alpha\nu\nu'}(t=0) = \delta C^{\sigma,\mathrm{eq}}_{\alpha\nu\nu'}(t=0), \tag{14}$$

$$\delta\hat{C}^{\sigma,\mathrm{RP}}_{\alpha\nu\nu'}(\omega=0) = \delta\hat{C}^{\sigma,\mathrm{eq}}_{\alpha\nu\nu'}(\omega=0), \tag{15}$$

$$\frac{d^n}{d\omega^n}\delta\hat{C}^{\sigma,\mathrm{RP}}_{\alpha\nu\nu'}(\omega=0) = \frac{d^n}{d\omega^n}\delta\hat{C}^{\sigma,\mathrm{eq}}_{\alpha\nu\nu'}(\omega=0). \tag{16}$$

These constraints extend the recently developed minimum-dissipaton ansatz,[54,55] which considers jointly the spectral density and Fermi function contributions. They ensure that the approximated correlations function, the spectrum, and its higher order derivatives maintain the exact values at $t = 0$ and $\omega = 0$, respectively. In other words, both the short-time and long-time behaviors of reservoir correlation functions have been properly taken into account.[54,55] Equations (14)–(16) further lead to

$$\begin{bmatrix} 1 & 1 & \cdots & 1 \\ \gamma_1^{-1} & \gamma_2^{-1} & \cdots & \gamma_R^{-1} \\ \vdots & \vdots & \ddots & \vdots \\ \gamma_1^{1-R} & \gamma_2^{1-R} & \cdots & \gamma_R^{1-R} \end{bmatrix} \begin{bmatrix} \eta^{\sigma}_{1} \\ \eta^{\sigma}_{2} \\ \vdots \\ \eta^{\sigma}_{R} \end{bmatrix} = \begin{bmatrix} S_{-1} \\ S_0 \\ \vdots \\ S_{R-2} \end{bmatrix}. \tag{17}$$

Here, S_{-1}, S_0, and S_k $(1 \le k \le R-2)$ come from Eqs. (14)–(16); see the Appendix for details. The involving matrix elements depend on the single parameter $\bar{\gamma}$ via Eq. (9). To determine this parameter, we minimize the quantity,

$$D^{\sigma}_{\alpha\nu\nu'}(\bar{\gamma}) = \int_0^\infty dt \left|\delta C^{\sigma,\mathrm{RP}}_{\alpha\nu\nu'}(t) - \delta C^{\sigma}_{\alpha\nu\nu'}(t)\right|^2, \tag{18}$$

by using Brent's algorithm.[58] Together with Eq. (17), the minimization of Eq. (18) provides a self-consistent determination of the parameters $\bar{\gamma}$ and $\{\eta^{\sigma}_{1}, \cdots, \eta^{\sigma}_{R}\}$. In the following calculations in Sec. IV, we first preset the total number of exponential terms $(P+1+R)$. Then we solve Eqs. (17) and (18) with all possible combinations of P and R and obtain the corresponding $D^{\sigma}_{\alpha\nu\nu'}(\bar{\gamma})$. The minimum value of $D^{\sigma}_{\alpha\nu\nu'}(\bar{\gamma})$ among all combinations gives the optimal choice of P and R.

We have thus completed the mixed PSD-LFLD expansion of the reservoir correlation function, $C^{\sigma,\mathrm{eq}}_{\alpha\nu\nu'}(t)$ in Eq. (7), into $(P + 1 + R)$ exponential terms. Together with the constraints, Eqs. (14)–(16) or equivalently Eq. (17), the logarithmic form of $\{\gamma_r\}$ in Eq. (9) provides a reasonable approximation for the exact spectrum in the low frequency regime, as will be shown below.

IV. RESULTS AND DISCUSSION

For the reservoir spectral function in Eq. (3), it is found that the real part of the reservoir correlation function Eq. (2) takes an exponential form of $\mathrm{Re}[C(t)] = \frac{\Delta W}{2} e^{-Wt}$; see the Appendix for details. Here, the indices $(\sigma\alpha\nu\nu')$ are omitted and we set $\sigma = +$. Therefore, the approximation is performed solely on the imaginary part $\mathrm{Im}[C(t)]$.

As depicted in Fig. 1(a), at the given temperature $T = 0.1\Delta$, a total number of $P + 1 + R = 6$ exponential terms for the LFLD scheme, i.e., $P = 2$ terms from the PSD scheme Eq. (5), 1 term from Eq. (3), and $R = 3$ terms adopted in Eq. (8), are enough to approximate the exact $\mathrm{Im}[C(t)]$, while for $P = 5$ in the PSD scheme, the curve significantly deviates from the exact one, and $P \ge 10$ is required to quantitatively reproduce the exact $\mathrm{Im}[C(t)]$. Also plotted are the real part of the approximated spectra $\mathrm{Re}[\hat{C}(\omega)]$ in Fig. 1(b). The LFLD scheme performs more accurate approximation than the PSD scheme with $P = 5$. It is noticed that $\mathrm{Re}[\hat{C}(\omega)]$ by the LFLD scheme might be slightly negative around $\omega \ge 0$, as shown in the inset. The negative $\mathrm{Re}[\hat{C}(\omega)]$ could occasionally lead to numerical inaccuracy in the long-time dynamics. Although

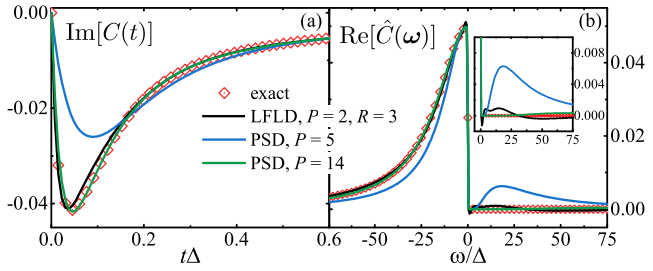

FIG. 1. The exact and approximated (a) imaginary part of the reservoir correlation function, Im[$C(t)$] and (b) real part of the spectrum, Re[$\hat{C}(\omega)$]. The inset magnifies Re[$\hat{C}(\omega)$] in $\omega \geq 0$. The parameters adopted are $W = 20\Delta$ and $T = 0.1\Delta$.

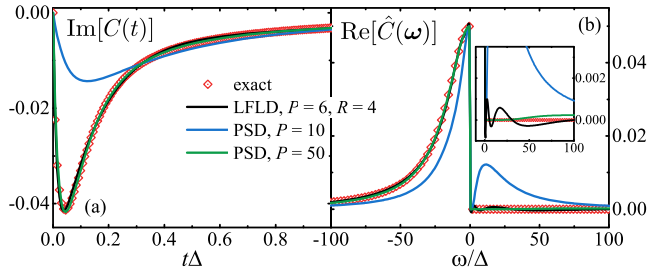

FIG. 3. The exact and approximated (a) imaginary part of the reservoir correlation function, Im[$C(t)$], and (b) real part of the spectrum, Re[$\hat{C}(\omega)$]. The inset magnifies Re[$\hat{C}(\omega)$] in $\omega \geq 0$. The parameters adopted are $W = 20\Delta$ and $T = 0.01\Delta$.

such a problem has not been found in our calculations, it has been observed in the long-time dynamics of the bilayer graphene system,[59] which could be a limitation of the LFLD scheme. However, it will not affect the evaluation of physical quantities in this work, as shown below.

The static and dynamic properties of the quantum impurity system are illustrated in Figs. 2(a) and 2(b), respectively. All the results are obtained at the truncation level $L = 4$ to ensure numerical convergence. Figure 2(a) plots the variation of the occupation (per spin) on the impurity n_s with the energy level ϵ_d in the equilibrium situation $V_\alpha = 0$. The HEOM calculated results with the LFLD scheme ($P = 2, R = 3$) show only minor discrepancies from the exact ones (PSD with $P = 14$). While the PSD scheme with $P = 5$ fails to predict the correct behaviors of n_s in the empty ($\epsilon_d > 0, n_\uparrow + n_\downarrow \sim 0$) and double ($\epsilon_d < -U$, $n_\uparrow + n_\downarrow \sim 2$) occupation regimes. In calculating n_s at each ϵ_d, the computational costs are the same for the LFLD ($P = 2$, $R = 3$) and PSD ($P = 5$) since the same number of exponential terms are adopted. In comparison, the physical memory and CPU time consumed by the standard PSD scheme with $P = 14$ are about 36 and 48 times larger, respectively. These observations show the superiority of the LFLD to the standard PSD at the same level of accuracy.

The dynamic properties evaluated with different schemes are examined in Fig. 2(b). A time-dependent voltage $V_\alpha(t) = V_{\alpha 0}(1 - e^{-t/t_c})$ is applied to α-reservoir ($\alpha = \mathrm{L}, \mathrm{R}$) at $t = 0$, with $V_{\alpha 0}$ being the amplitude and t_c the characteristic time; see the inset of Fig. 2(b). The energy level is set to $\epsilon_d = -4\Delta$ so that the system is in the strongly correlated Kondo regime. The transient current $I_\mathrm{L}(t)$ is then plotted. The curve obtained with the LFLD scheme ($P = 2$, $R = 3$) agrees remarkably well with the exact result with a relative error ~3%, when the system evolves to steady state. Although the PSD scheme with $P = 5$ gives plausible results in the single occupation ($-U < \epsilon_d < 0, n_\uparrow + n_\downarrow \sim 1$) regime in Fig. 2(a), the corresponding transient current deviates a lot from the exact results, as depicted in Fig. 2(b). These observations affirm that the proposed LFLD scheme applies well even in the Kondo-correlated regime.

The superiority of the proposed LFLD scheme over the PSD scheme is more clear when the temperature is lowered to $T = 0.01\Delta$. As depicted in Fig. 3, to accurately reproduce the exact Im[$C(t)$], the number of exponential terms needed in the PSD scheme is $P + 1 = 51$, while it is only $P + 1 + R = 11$ in the LFLD scheme. The real part of the spectrum Re[$\hat{C}(\omega)$] by the LFLD scheme also agrees well with the exact one, albeit the negative values around $\omega \geq 0$. Therefore, the newly proposed LFLD scheme will greatly reduce the number of ADOs in each tier[34,39] and facilitate the efficient implementation of the HEOM approach.

We now evaluate the occupation n_s and transient current $I_\mathrm{L}(t)$ with the aforementioned two schemes. At such a low temperature $T = 0.01\Delta$, the hierarchy in Eq. (6) should be truncated at the level $L \geq 4$ to obtain the quantitatively converged results for the interacting systems ($U > 0$). Although the LFLD scheme would be equally applicable to the interacting system, the computational cost will increase drastically for the PSD scheme with $P = 50$, which is much beyond the resources at our disposal. Therefore, we choose to investigate the static and dynamic properties of a noninteracting system ($U = 0$). In this case,[20,34,39,60] the hierarchy terminates automatically and exactly at $L = 2$ for the determination of any single-electron properties, and the computational

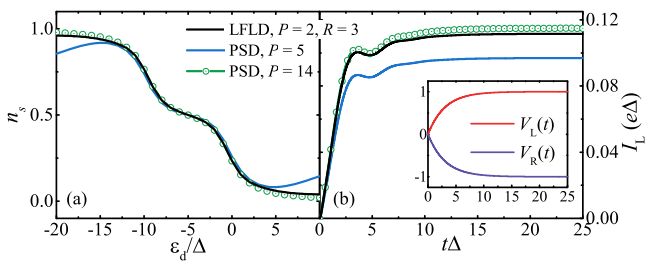

FIG. 2. (a) The calculated occupation n_s ($s = \uparrow$ or $\downarrow$) versus the energy level ϵ_d. (b) The transient current $I_\mathrm{L}(t)$ versus time t, with $\epsilon_d = -4\Delta$, $t_c = 3/\Delta$, and $V_{\mathrm{L}0} = -V_{\mathrm{R}0} = \Delta$. The inset plots the corresponding voltage versus time. Other parameters adopted are $\Delta_\mathrm{L} = \Delta_\mathrm{R} = 0.5$, $U = 10\Delta$, $W = 20\Delta$, and $T = 0.1\Delta$.

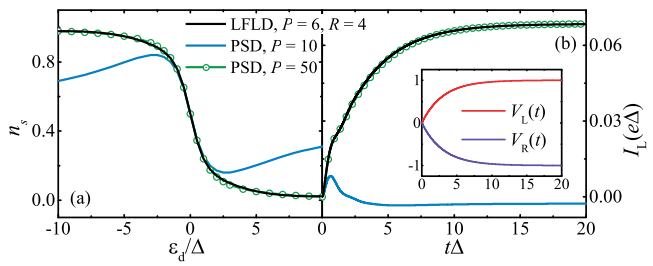

FIG. 4. (a) The calculated occupation n_s ($s = \uparrow$ or $\downarrow$) versus the energy level ϵ_d. (b) The transient current $I_\mathrm{L}(t)$ versus time t, with $\epsilon_d = -3\Delta$, $t_c = 3/\Delta$, and $V_{\mathrm{L}0} = -V_{\mathrm{R}0} = \Delta$. The inset plots the corresponding voltage versus time. Other parameters adopted are $\Delta_\mathrm{L} = \Delta_\mathrm{R} = 0.5$, $U = 0$, $W = 20\Delta$, and $T = 0.01\Delta$.

cost will be appreciably alleviated. As depicted in Fig. 4, numerically exact results are given by the PSD scheme with $P = 50$. Both the equilibrium occupation n_s and transient current $I_L(t)$ by the LFLD scheme ($P = 6$, $R = 4$) agree perfectly with the exact results. This clearly verifies the feasibility and effectiveness of the LFLD scheme for the decomposition of the reservoir spectrum even in the extremely low temperature regime.

V. CONCLUDING REMARKS

To conclude, we have proposed a LFLD scheme for the efficient decomposition of the fermionic reservoir spectrum. The present scheme combines the advantages of the PSD scheme[24,40,53] and the minimum-dissipaton ansatz.[54,55] This scheme is applicable to the general sum-over-poles form of spectral density. While PSD treats the Fermi function and the spectral density function separately, the extended minimum-dissipaton ansatz, Eqs. (14)–(16), handles these two functions jointly in the residual term. It is shown that the proposed LFLD scheme exhibits significant superiority over the PSD scheme as the reservoir temperature lowers. More importantly, the new scheme goes also by the intuitive consideration of logarithmic discretization of Eq. (9). This remarkably insightful form of $\{\gamma_r\}$, characterized by a single characteristic scaling parameter $\bar{\gamma}$, is applicable even to the extremely low temperature regime, as numerically demonstrated in this work. While Eq. (14) assures the short-time accuracy, Eqs. (15) and (16) dictate the long-time accuracy, covering the memory time up to $10^{R-1}/\bar{\gamma}$. The LFLD coefficients $\{\eta_r^\sigma\}$ and parameter $\bar{\gamma}$ are then determined under the constraints of Eqs. (14)–(16), or equivalently Eq. (17), together with the minimization of Eq. (18). The proposed method effectively captures the low-frequency features that are of pivotal influence on the system properties at low temperatures. While a minimum-dissipaton ansatz for the decomposition of the bosonic bath spectrum has been proposed,[54,55] it is anticipated that the LFLD scheme is also applicable to the optimal construction of the bosonic HEOM formalism at extremely low temperatures.

The optimized HEOM approach in conjunction with the LFLD scheme is then employed to investigate the static and dynamic properties of quantum impurity systems. Numerical simulation results show remarkable agreement with the PSD based ones in both the Kondo-correlated and noninteracting regimes, while the computational cost is substantially reduced with a much smaller number of exponential terms in Eq. (4). It is anticipated that the LFLD scheme will greatly facilitate the accurate HEOM-based studies in various problems such as Kondo phenomena in multi-impurity systems in extremely low temperature regimes.

ACKNOWLEDGMENTS

The support from the Ministry of Science and Technology (Nos. 2016YFA0400900 and 2016YFA0200600), Natural Science Foundation of China (Nos. 21233007, 21373191, 21573202, and 21633006), the Fundamental Research Funds for the Central Universities (Nos. 2030020028, 2340000074, and WK2060030025), and the Anhui Provincial Natural Science Foundation (No. 1708085QB30) is gratefully acknowledged.

APPENDIX: DETERMINE THE $\{S_k\}$-PARAMETERS

Substituting Eqs. (3) and (5) into Eq. (2) and utilizing the contour integral technique lead to

$$C_{\alpha\nu\nu'}^{\sigma,\mathrm{PSD}}(t) = \frac{\Delta_\alpha W}{2} e^{-Wt} - i\frac{2\Delta_\alpha W^2}{\beta_\alpha} \times \sum_{p=1}^{P} \frac{\tilde{\eta}_p}{\tilde{\xi}_p^2 - W^2}\left(e^{-Wt} - e^{-\tilde{\xi}_p t}\right). \tag{A1}$$

It reduces to the conventional MSD scheme and recovers the exact reservoir correlation function $C_{\alpha\nu\nu'}^{\sigma,\mathrm{eq}}(t)$ when $P \to \infty$. It is straightforward to see that the real part of $C_{\alpha\nu\nu'}^{\sigma,\mathrm{eq}}(t)$ is $\frac{\Delta W}{2} e^{-Wt}$ since the coefficients $\{\tilde{\eta}_p\}$ and $\{\tilde{\xi}_p\}$ are all real numbers.[24,53]

The spectra defined in Eqs. (12) and (13) can be evaluated as

$$\begin{aligned}\delta\hat{C}_{\alpha\nu\nu'}^{\sigma,\mathrm{eq}}(\omega) &= -i\frac{2\Delta_\alpha W}{\beta_\alpha}\Bigg[\sum_{p=1}^{\infty}\frac{\tilde{\eta}'_p}{\tilde{\xi}'^2_p - W^2}\left(\frac{1}{W+\sigma i\omega} - \frac{1}{\tilde{\xi}'_p + \sigma i\omega}\right) \\ &\quad - \sum_{p=1}^{P}\frac{\tilde{\eta}_p}{\tilde{\xi}_p^2 - W^2}\left(\frac{1}{W+\sigma i\omega} - \frac{1}{\tilde{\xi}_p + \sigma i\omega}\right)\Bigg], \end{aligned}\tag{A2}$$

$$\delta\hat{C}_{\alpha\nu\nu'}^{\sigma,\mathrm{RP}}(\omega) = \sum_{r=1}^{R}\frac{\eta_r^\sigma}{\gamma_r + \sigma i\omega}. \tag{A3}$$

The second line in Eq. (A2) comes from the exact $C_{\alpha\nu\nu'}^{\sigma,\mathrm{eq}}(t)$, and the third line comes from $C_{\alpha\nu\nu'}^{\sigma,\mathrm{PSD}}(t)$. Equations (14)–(16) can be cast into the compact form of

$$\begin{aligned} S_k &\equiv \sum_{r=1}^{R}\frac{\eta_r^\sigma}{\gamma_r^{k+1}} \\ &= -i\frac{2\Delta_\alpha W^2}{\beta_\alpha}\Bigg[\sum_{p=1}^{\infty}\frac{\tilde{\eta}'_p}{\tilde{\xi}'^2_p - W^2}\left(\frac{1}{W^{k+1}} - \frac{1}{\tilde{\xi}'^{k+1}_p}\right) \\ &\quad - \sum_{p=1}^{P}\frac{\tilde{\eta}_p}{\tilde{\xi}_p^2 - W^2}\left(\frac{1}{W^{k+1}} - \frac{1}{\tilde{\xi}_p^{k+1}}\right)\Bigg]. \end{aligned}\tag{A4}$$

This is just Eq. (17).

[1] K. G. Wilson, Rev. Mod. Phys. **47**, 773 (1975).
[2] R. Bulla, T. A. Costi, and T. Pruschke, Rev. Mod. Phys. **80**, 395 (2008).
[3] S. R. White, Phys. Rev. Lett. **69**, 2863 (1992).
[4] J. E. Hirsch and R. M. Fye, Phys. Rev. Lett. **56**, 2521 (1986).
[5] E. Gull, A. J. Millis, A. I. Lichtenstein, A. N. Rubtsov, M. Troyer, and P. Werner, Rev. Mod. Phys. **83**, 349 (2011).
[6] M. Caffarel and W. Krauth, Phys. Rev. Lett. **72**, 1545 (1994).
[7] S. Weiss, J. Eckel, M. Thorwart, and R. Egger, Phys. Rev. B **77**, 195316 (2008).
[8] L. Mühlbacher and E. Rabani, Phys. Rev. Lett. **100**, 176403 (2008).
[9] H. D. Meyer, U. Manthe, and L. S. Cederbaum, Chem. Phys. Lett. **165**, 73 (1990).
[10] H. B. Wang and M. Thoss, J. Chem. Phys. **119**, 1289 (2003).
[11] Y. Tanimura and R. Kubo, J. Phys. Soc. Jpn. **58**, 101 (1989).
[12] Y. Tanimura, Phys. Rev. A **41**, 6676 (1990).
[13] Y. Tanimura and P. G. Wolynes, Phys. Rev. A **43**, 4131 (1991).

[14]Y. Tanimura and S. Mukamel, J. Phys. Soc. Jpn. **63**, 66 (1994).
[15]Y. A. Yan, F. Yang, Y. Liu, and J. S. Shao, Chem. Phys. Lett. **395**, 216 (2004).
[16]A. Ishizaki and Y. Tanimura, J. Phys. Soc. Jpn. **74**, 3131 (2005).
[17]Y. Tanimura, J. Phys. Soc. Jpn. **75**, 082001 (2006).
[18]R. X. Xu, P. Cui, X. Q. Li, Y. Mo, and Y. J. Yan, J. Chem. Phys. **122**, 041103 (2005).
[19]R. X. Xu and Y. J. Yan, Phys. Rev. E **75**, 031107 (2007).
[20]J. S. Jin, X. Zheng, and Y. J. Yan, J. Chem. Phys. **128**, 234703 (2008).
[21]X. Zheng, J. S. Jin, S. Welack, M. Luo, and Y. J. Yan, J. Chem. Phys. **130**, 164708 (2009).
[22]M. Tanaka and Y. Tanimura, J. Phys. Soc. Jpn. **78**, 073802 (2009).
[23]C. Kreisbeck, T. Kramer, M. Rodríguez, and B. Hein, J. Chem. Theory Comput. **7**, 2166 (2011).
[24]J. Hu, M. Luo, F. Jiang, R. X. Xu, and Y. J. Yan, J. Chem. Phys. **134**, 244106 (2011).
[25]J. Strümpfer and K. Schulten, J. Chem. Theory Comput. **8**, 2808 (2012).
[26]C. Kreisbeck and T. Kramer, J. Phys. Chem. Lett. **3**, 2828 (2012).
[27]Y. Tanimura, J. Chem. Phys. **137**, 22A550 (2012).
[28]Z. H. Li, N. H. Tong, X. Zheng, D. Hou, J. H. Wei, J. Hu, and Y. J. Yan, Phys. Rev. Lett. **109**, 266403 (2012).
[29]J. M. Moix and J. Cao, J. Chem. Phys. **139**, 134106 (2013).
[30]Y. Jing, L. Chen, S. Bai, and Q. Shi, J. Chem. Phys. **138**, 01B615 (2013).
[31]R. Härtle, G. Cohen, D. R. Reichman, and A. J. Millis, Phys. Rev. B **88**, 235426 (2013).
[32]C. Kreisbeck, T. Kramer, and A. Aspuru-Guzik, J. Chem. Theory Comput. **10**, 4045 (2014).
[33]H. Liu, L. Zhu, S. Bai, and Q. Shi, J. Chem. Phys. **140**, 134106 (2014).
[34]D. Hou, S. K. Wang, R. L. Wang, L. Z. Ye, R. X. Xu, X. Zheng, and Y. J. Yan, J. Chem. Phys. **142**, 104112 (2015).
[35]M. Tsuchimoto and Y. Tanimura, J. Chem. Theory Comput. **11**, 3859 (2015).
[36]K. Song, S. Bai, and Q. Shi, J. Chem. Phys. **143**, 064109 (2015).
[37]Z. Tang, X. Ouyang, Z. Gong, H. Wang, and J. Wu, J. Chem. Phys. **143**, 224112 (2015).
[38]J. Wu, Z. Gong, and Z. Tang, J. Chem. Phys. **143**, 074102 (2015).
[39]L. Z. Ye, X. L. Wang, D. Hou, R. X. Xu, X. Zheng, and Y. J. Yan, Wiley Interdiscip. Rev.: Comput. Mol. Sci. **6**, 608 (2016).
[40]Y. J. Yan, J. S. Jin, R. X. Xu, and X. Zheng, Front. Phys. **11**, 110306 (2016).
[41]J.-i. Okamoto, L. Mathey, and R. Härtle, Phys. Rev. B **94**, 235411 (2016).
[42]M. Xu, L. Song, K. Song, and Q. Shi, J. Chem. Phys. **146**, 064102 (2017).
[43]Y. Wang, X. Zheng, B. Li, and J. L. Yang, J. Chem. Phys. **141**, 084713 (2014).
[44]Y. Wang, X. Zheng, and J. L. Yang, Phys. Rev. B **93**, 125114 (2016).
[45]Y. Wang, X. Zheng, and J. L. Yang, J. Chem. Phys. **145**, 154301 (2016).
[46]X. L. Wang, D. Hou, X. Zheng, and Y. J. Yan, J. Chem. Phys. **144**, 034101 (2016).
[47]D. Hou, R. L. Wang, X. Zheng, N. H. Tong, J. H. Wei, and Y. J. Yan, Phys. Rev. B **90**, 045141 (2014).
[48]L. Z. Ye, D. Hou, R. L. Wang, D. W. Cao, X. Zheng, and Y. J. Yan, Phys. Rev. B **90**, 165116 (2014).
[49]L. Z. Ye, D. Hou, X. Zheng, Y. J. Yan, and M. Di Ventra, Phys. Rev. B **91**, 205106 (2015).
[50]L. Z. Ye, X. Zheng, Y. J. Yan, and M. Di Ventra, Phys. Rev. B **94**, 245105 (2016).
[51]A. Erpenbeck, R. Härtle, M. Bockstedte, and M. Thoss, Phys. Rev. B **93**, 115421 (2016).
[52]T. Ozaki, Phys. Rev. B **75**, 035123 (2007).
[53]J. Hu, R. X. Xu, and Y. J. Yan, J. Chem. Phys. **133**, 101106 (2010).
[54]J. J. Ding, H. D. Zhang, Y. Wang, R. X. Xu, X. Zheng, and Y. J. Yan, J. Chem. Phys. **145**, 204110 (2016).
[55]J. J. Ding, Y. Wang, H. D. Zhang, R. X. Xu, X. Zheng, and Y. J. Yan, J. Chem. Phys. **146**, 024104 (2017).
[56]A. Croy and U. Saalmann, Phys. Rev. B **80**, 073102 (2009).
[57]X. Zheng, R. X. Xu, J. Xu, J. S. Jin, J. Hu, and Y. J. Yan, Prog. Chem. **24**, 1129 (2012), http://www.progchem.ac.cn/EN/Y2012/V24/I06/1129.
[58]R. P. Brent, *Algorithms for Minimization Without Derivatives* (Prentice Hall, New Jersey, 1973), ISBN: 0-13-022335-2.
[59]R. Wang, X. Zheng, Y. Kwok, H. Xie, G. Chen, and C. Yam, J. Chem. Phys. **142**, 144112 (2015).
[60]X. Zheng, Y. J. Yan, and M. Di Ventra, Phys. Rev. Lett. **111**, 086601 (2013).